J. Phys. Chem. **1988,** *92,* 4184–4190

a direct consequence of the fact that both C–H bond lengths are also very similar.

For insight into the description of the electronic structure of the transition state, Figure 5 presents the spin density map. Obviously, in the reactants the spin density differs from zero only on triplet methylene, since ethylene is a closed-shell molecule. Figure 5 shows that the α spin density of triplet methylene has been delocalized over the whole system at the transition state. In ethylene the α spin density is concentrated on the carbon atom that is closest to methylene. Another interesting fact is the existence of a noticeable β spin density at the hydrogen atom that is being transferred. This is due to an important phenomenon of spin polarization in the linear fragment C–H–C.

Let us now compare the results obtained for the two studied processes. Undoubtedly, the most important difference between them lies in the values of the energy barriers. Thus, the energy barrier for the insertion reaction of singlet methylene is much smaller than the one corresponding to hydrogen abstraction by triplet methylene. This occurs at all levels of calculation considered by us. At the MP3/6-31G*//3-21G level, for instance, the hydrogen abstraction by triplet methylene requires a barrier of 24.4 kcal/mol while no energy barrier is found for the insertion reaction of singlet methylene. In fact this great difference between both energy barriers mainly arises from the energy gap between singlet and triplet methylene, this gap being 18.5 kcal/mol at the MP3/6-31G*//3-21G level of calculation.

Regarding, the mechanism, it is generally accepted that the insertion of singlet methylene takes place in one step via formation of a cyclic tricentric bond, while triplet methylene abstracts one hydrogen atom in a first step, the subsequent formation of a C–C bond between the two generated radicals requiring a previous intersystem crossing. Our results seem to indicate that both processes are not very different at the beginning, since the structure of the transition state for the insertion of singlet methylene does not present such a cyclic tricentric bond, and the main component of the transition vector corresponds to the transfer of one hydrogen atom from ethylene to methylene.

Finally, another aspect that is interesting to discuss is the competition between the studied processes and the addition of singlet and triplet methylene to the ethylenic double bond. It is well-known that the insertion of singlet methylene into vinylic C–H bonds can compete with the addition process, although the latter is faster.[5,49] On the contrary, the hydrogen abstraction by triplet methylene is never observed when addition to a double bond is also possible.[50] All these facts can be understood if one compares the energy barriers obtained in this work with those previously calculated for the addition of singlet[51,52] and triplet[48] methylene to ethylene. Thus, the competition in the case of singlet methylene can be explained by the facts that no energy barrier is found for the addition process at all levels of calculation and the same occurs for insertion when electron correlation is introduced. On the contrary, the addition of triplet methylene has a much smaller energy barrier than the one corresponding to the hydrogen abstraction process. For instance, the energy barriers are 11.2 and 25.7 kcal/mol, respectively, at the MP2/3-21G//3-21G level of calculation. This large difference is the responsible for the fact that the hydrogen abstraction reaction is not observed when addition to a double bond is possible.

In conclusion, we believe that this work has permitted us to gain insight into the different reactivity patterns that present singlet and triplet methylene when they react in front of a vinylic double bond. In the first stage both processes imply the transfer of a hydrogen atom from ethylene to methylene, this transfer being already important at the transition state. Given this similarity between the structures of both transition states, the difference in the energy barriers mainly arises from the energy gap between singlet and triplet methylene. Finally, the results obtained in this work have also permitted us to understand the different competitivity of the two studied processes when compared with the well-known addition reactions to olefinic double bonds.

Acknowledgment. This work has been supported by the U. S.–Spain Joint Committee for Scientific and Technological Cooperation under Contract No. CCB-8509/016.

Registry No. Methylene, 2465-56-7; ethylene, 74-85-1.

---

(49) Tomioka, H.; Tabayashi, K.; Ozaki, Y.; Izawa, Y. *Tetrahedron* **1985,** *41,* 1435.

(50) Ring, D. F.; Rabinovitch, B. S. *Can. J. Chem.* **1968,** *46,* 2435.

(51) Zurawski, B.; Kutzelnigg, W. *J. Am. Chem. Soc.* **1978,** *100,* 2654.

(52) Rondan, N. G.; Houk, K. N.; Moss, R. A. *J. Am. Chem. Soc.* **1980,** *102,* 1770.

Pressure and Temperature Dependence of the Gas-Phase Recombination of Hydroxyl Radicals

R. Zellner,* F. Ewig, R. Paschke, and G. Wagner

Institut für Physikalische Chemie, Universität Göttingen, Tammannstrasse 6, 3400 Göttingen, FRG

(Received: August 28, 1987)

Rate constants for the reaction $OH + OH + M \rightarrow H_2O_2 + M$ ($M = N_2, H_2O$) have been determined by using flash photolysis of H_2O vapor in combination with quantitative OH resonance spectrometry. For $M = N_2$ experiments were performed at 253, 298, and 353 K and at pressures between 26 and 1100 mbar. Under these conditions the reaction is found to be primarily in the low-pressure limit with $k_{1,N_2}{}^0$ (T = 298 K) = $(6.9^{+1.4}_{-2.5}) \times 10^{-31}$ cm^6/s and a temperature dependence of $T^{-0.8}$. Both the absolute value of $k_{1,N_2}{}^0$ and its temperature variation are in very satisfactory agreement with theoretical predictions and extrapolations from high-temperature dissociation data. A pressure falloff of k_{1,N_2} is also observed. On the basis of a theoretical analysis of the falloff behavior, a high-pressure limiting rate coefficient of $k_1{}^\infty = 1.5 \times 10^{-11}$ cm^3/s, independent of temperature, is predicted. From experiments in N_2/H_2O mixtures with $x_{H_2O} = 0.11$ at pressures up to 140 mbar a low-pressure limiting rate coefficient for H_2O as a third body of $k_{1,H_2O}{}^0$ (T = 298 K) = $(4.0^{+1.3}_{-2.0}) \times 10^{-30}$ cm^6/s is obtained.

I. Introduction

Due to their importance in the chemistry of combustion processes and in the atmosphere, reactions of OH radicals have received considerable attention. The range of interest covers the temperature region from around 250 K up to 2000 K and the pressure scale from a few millibars to 1 bar. Although considerable progress has been made in recent years in measuring the rate coefficients for bimolecular reactions of the OH radical, comparatively little work has been devoted to a study of the termolecular process

0022-3654/88/2092-4184$01.50/0

$$OH + OH (+M) \rightarrow H_2O_2 (+M) \qquad \Delta H_R = -215 \text{ kJ/mol} \tag{1}$$

This recombination of OH radicals is in competition with the corresponding disproportionation, viz.

$$OH + OH \rightarrow H_2O + O \qquad \Delta H_R = -71 \text{ kJ/mol} \tag{2}$$

In fact reaction 2 is sufficiently exothermic to create a dominantly bimolecular flux and hence to suppress recombination provided both reactions occurred via a common intermediate on the same electronic potential surface. This, however, is not the case since the interaction of two OH($^2\Pi$) radicals gives rise to both singlet and triplet surfaces which keep the product channels (1) and (2) separated.

Despite their molecular separation, reactions 1 and 2 always occur simultaneously, and formidable difficulties arise in their experimental isolation. Whereas this has been achieved for reaction 2 by use of low-pressure studies[1-6] or corresponding extrapolations,[7,8] the same is not the case for reaction 2. The recombination of OH radicals was first studied by Black and Porter[9] using absorption spectrometry in the flash photolysis of H_2O vapor and up to 1 bar of various third bodies. In similar flash mixtures Caldwell and Back[10] subsequently monitored the yields of H_2 and O_2 and obtained estimates for the relative rates of reactions 1 and 2. Together with the relative third-body efficiencies as determined by Black and Porter[9] and the absolute value of k_2 as obtained by Del Greco and Kaufman,[1] this provided the first indirect information on the rate coefficient k_1. The only direct study of reaction 1 was performed by Trainor and von Rosenberg[7] using flash photolysis in combination with quantitative line spectrometry. From measurements in up to 520 mbar of N_2 these authors obtained a rate coefficient in the low-pressure limit of k_1^0 (M = N_2) = (2.5 ± 0.3) × 10^{-31} cm^6/s; a pressure falloff, however, was not observed.

The present work is both a refinement and extension of the work of ref 7 using essentially the same experimental technique. Moreover, since we have observed the falloff behavior of reaction 1, our data are being analyzed in terms of current unimolecular rate theory. A comparison with high-temperature dissociation data is also provided.

II. Experimental Section

The reaction has been studied by using a conventional flash photolysis technique to generate OH in a mixture of N_2/H_2O ($H_2O + h\nu$ ($\lambda \leq 185$ nm) $\rightarrow$ OH($^2\Pi$) + H(^2S)) and by observing the time-resolved decay of OH using quantitative resonance absorption in the rotational lines of the $A^2\Sigma^+-X^2\Pi-(0,0)$-band transition. The technique has been described fully,[8,11,12] and only the main features and necessary modifications will be briefly mentioned.

The Spectrosil quartz reaction cell (length, 600 mm; inner diameter, 36 mm) and the flash lamp are of annular arrangement. Both together are surrounded by a third tube through which oil—either from a cryostat or from a thermostat—can be circulated. The accessible temperature range is 250–400 K. The end windows of the reaction cell are placed well inside the thermostated and flash-illuminated region at a mutual distance (equal to the absorption path length) of 370 mm. This arrangement not only ensures a homogeneous temperature profile along the reactor, it also avoids larger axial concentration gradients of OH which cannot be accepted in second-order kinetics. The detection of OH is along the axial direction. Moreover, due to the short absorption path length relatively high OH concentrations ($\geq 10^{14}$ cm^{-3}) can be used without creating undue large and nonlinear absorptions.[8]

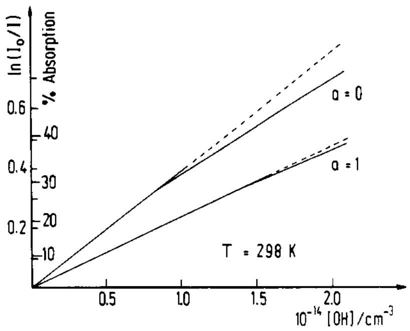

Figure 1. Calculated line absorption intensity as a function of OH concentration (T = 300 K, l = 37 cm, $Q_1$4 line) for (i) pure Doppler line shape (a = 0) and (ii) combined Doppler- and pressure-broadened lines (a = 1). The line oscillator strength is taken as 5.2. × 10^{-4}; the emitter temperature is assumed to be 650 K.[11] In each case the dotted line represents the small absorption limit.

TABLE I: Effective Absorption Coefficients of the $Q_1$4 Line of the $A^2\Sigma^+$, v' = 0 → $X^2\Pi$, v'' = 0 Transition of OH for Pure Doppler Profile (ϵ_D) and Corresponding Pressure Corrections

	$f(p)$		
p/mbar	253 K	298 K	353 K
0	1.0	1.0	1.0
130	0.94	0.95	0.95
260	0.83	0.85	0.86
390	0.74	0.76	0.78
520	0.67	0.69	0.72
650	0.66	0.67	0.69
780	0.62	0.63	0.65
910	0.59	0.60	0.62
1040	0.57	0.58	0.60
ϵ_D/cm^2	9.49 × 10^{-17}	1.06 × 10^{-16}	1.12 × 10^{-16}

In experiments with N_2 as a third body the H_2O partial pressure was between 0.5 and 0.8 mbar for all pressures up to 1100 mbar. In experiments to determine the rate coefficient for recombination with H_2O as a third body, mixtures of N_2 and H_2O with a mole fraction of x_{H_2O} = 0.11 at total pressures up to 140 mbar were used.

Effective OH Absorption Coefficients for Combined Temperature- and Pressure-Broadened Lines. In order to analyze absorption vs time profiles in second-order kinetics, absolute OH concentrations have to be known. These can be obtained from the observed absorptions by using quantitative line absorption spectrometry. According to theory[13,14] the absorption (A) resulting from a resonance transition ($A^2\Sigma^+$, v' = 0, $J' \rightarrow X^2\Pi$, v'' = 0, J'') of the OH radical will be given by

$$A = \frac{\int I_\nu^0[1 - \exp(-f(\nu)\epsilon_0[\text{OH}]l)]\,d\nu}{\int I_\nu^0\,d\nu} \tag{i}$$

where I_ν^0 is the line intensity distribution of the light source, ϵ_0 is the absorption coefficient in the center of a Doppler-broadened line

$$\epsilon_0 = ((\ln 2)/\pi)^{1/2}(2\pi e^2/mc\Delta\nu_D f_{J'J''}) \times (2J'' + 1)\exp(-E_{J''}/RT)/Q_{\text{Rot}} \tag{ii}$$

and $f(\nu)$ is the line shape factor. For a pure Doppler profile of the absorber

$$f(\nu) = \exp\{-[2(\nu - \nu_0)(\ln 2)^{1/2}/\Delta\nu_D]^2\} \tag{iii}$$

---

(1) Del Greco, F. P.; Kaufman, F. *Discuss. Faraday Soc.* **1962**, *33*, 128.

(2) Dixon-Lewis, G.; Wilson, W. E.; Westenberg, A. A. *J. Chem. Phys.* **1966**, *44*, 2877.

(3) Breen, J. E.; Glass, J. P. *J. Chem. Phys.* **1970**, *52*, 1082.

(4) Westenberg, A. A.; de Haas, N. *J. Chem. Phys.* **1973**, *58*, 4006.

(5) McKenzie, A.; Mulcahy, M. F. R.; Steven, J. R. *J. Chem. Phys.* **1973**, *59*, 3244.

(6) Clyne, M. A. A.; Down, S. *J. Chem. Soc., Faraday Trans. 2* **1974**, *70*, 253.

(7) Trainor, D. W.; von Rosenberg, C. W. *J. Chem. Phys.* **1974**, *61*, 1010.

(8) Wagner, G.; Zellner, R. *Ber. Bunsen-Ges. Phys. Chem.* **1981**, *85*, 1122.

(9) Black, G.; Porter, G. *Proc. R. Soc. London, A* **1962**, *266*, 185.

(10) Caldwell, J.; Back, R. A. *Trans. Faraday Soc.* **1965**, *61*, 1939.

(11) Zellner, R.; Steinert, W.; *Int. J. Chem. Kinet.* **1976**, *8*, 397.

(12) Handwerk, V.; Zellner, R. *Ber. Bunsen-Ges. Phys. Chem.* **1978**, *82*, 1161.

(13) Mitchell, A. C. G.; Zemansky, M. *Resonance Radiation and Excited Atoms*; Cambridge University Press: Cambridge, U.K., 1961.

(14) Penner, S. S. *Quantitative Molecular Spectroscopy and Gas Emissivities*; Addison-Wesley: Reading, MA, 1959.

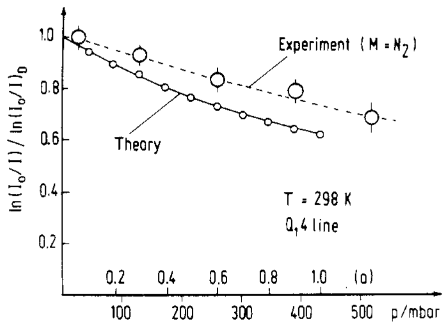

Figure 2. Comparison of experimental (M = N_2) and theoretical pressure corrections of absorption intensities for constant OH concentrations. T = 298 K, Q_14 line. The theoretical curve is calculated as a function of a, the relative line broadening coefficient.

and emitter, eq i can be solved explicitly. In the limit of small absorptions one obtains[8]

$$A = (5.11 \times 10^{-6}) \times [\mathrm{OH}]l\{(2J'' + 1)f_{J'J''}/\nu_0\} \exp(-E_{J''}/RT)/Q_{\mathrm{Rot}}(T_E + T_A)^{1/2} \quad \text{(iv)}$$

where T_E and T_A are the temperatures of the emitter (resonance lamp) and absorber, respectively. The resulting absorption as a function of [OH] from eq iv and for the full solution of eq i and eq iii is shown in Figure 1. The corresponding absorption coefficient $\epsilon_D = A/[\mathrm{OH}]l$ is tabulated (Table I).

In the case of combined Doppler and pressure broadening $f(\nu)$ assumes a Voigt profile, viz.

$$f(\nu) = (a/\pi)\int \frac{\exp(-y^2)\,\mathrm{d}y}{a^2 + [2(\nu - \nu_0)(\ln 2)^{1/2}/\Delta\nu_D - y]^2} \quad \text{(v)}$$

In here a is the relative line width associated with the two broadening mechanisms, $a = (\Delta\nu_L/\Delta\nu_D)(\ln 2)^{1/2}$. Equations i and v can be solved numerically with approximate expressions[13] for $f(\nu)$. A typical result for comparable extent of pressure and Doppler broadening (a = 1) is shown in Figure 1. As can be seen, the resulting absorption intensities for constant [OH] are reduced to about 60% of the values predicted for pure Doppler line shapes (a = 0).

The above calculation to predict pressure-dependent corrections for the effective OH absorption coefficient is only useful if the connection of a (or $\Delta\nu_L$) with pressure is explicitly known. This, however, is not the case because the cross section for collisional line broadening is not known a priori. Therefore, we have adopted a purely experimental method to derive the pressure correction by performing measurements of the initial OH absorption at different total pressures but for otherwise identical conditions. The result for T = 298 K is shown in Figure 2. As can be seen, the pressure correction is essential ($\geq$5%) for all N_2 pressures above 100 mbar. Pressure correction factors $f(p)$ are summarized in Table I.

Figure 2 also contains the result of a computation of the initial absorption for different values of a. By comparison with the experiment it is found that, for instance, a pressure of 520 mbar of N_2 corresponds to a = 0.7. Using the definition $a = (\Delta\nu_L/\Delta\nu_D)(\ln 2)^{1/2}$ and the theoretical expression

$$\Delta\nu_L = (2/\pi)\sigma_L^2[\mathrm{N}_2]\{2RT(M_1^{-1} + M_2^{-1})\}^{1/2} \quad \text{(vi)}$$

a collisional line broadening cross section of $\sigma_L^2 = 2.5 \times 10^{-15}$ cm^2 can be derived. Equation vi has also been used to derive the temperature dependence of the pressure correction factor $f(p)$ (see Table I). No particular account has been taken for the influence of H_2O vapor on the line broadening corrections.

III. Results and Discussion

III.1. Pressure and Temperature Dependence of the Recombination Rate Coefficient. III.1.1. $M = N_2$. Following the flash photolysis of H_2O vapor in N_2 as a diluent we observe second-order decays of OH radicals. A representative example of OH absorption vs time together with the corresponding second-order analysis is shown in Figure 3. From the slope of this line the effective second-order rate coefficient k_{eff}, defined by $k_{\mathrm{eff}} = -\mathrm{d}[\mathrm{OH}]/[\mathrm{OH}]^2\,\mathrm{d}t$, is obtained as

$$k_{\mathrm{eff}} = (1/\Delta[\mathrm{OH}])/\Delta t = \{\epsilon_D f(p) l/\Delta \ln (I_0/I)\}/\Delta t$$

It is found that k_{eff} changes strongly with N_2 pressure but is only moderately dependent on temperature (Figure 4). Experimental conditions and results are summarized in Table II.

TABLE II: Summary of Experimental Conditions and Results for M = N_2

T/K	p/mbar	no. expt	$10^{12}k_{\mathrm{eff}}$/cm^3 s^{-1}	$10^{12}k_1$/cm^3 s^{-1}
253	26	10	4.2 ± 0.6	0.56 ± 0.15
	52	9	5.3 ± 1.0	1.1 ± 0.25
	79	9	6.2 ± 1.4	1.6 ± 0.4
	92	11	7.0 ± 1.3	1.9 ± 0.5
	105	7	6.5 ± 2.0	1.7 ± 0.6
	131	17	7.4 ± 1.5	2.1 ± 0.6
	262	8	10.6 ± 2.1	3.8 ± 1.0
	393	10	10.7 ± 2.8	3.8 ± 1.2
	526	7	11.0 ± 2.8	4.0 ± 1.4
	526	7	11.8 ± 2.9	4.3 ± 1.6
	657	8	12.8 ± 3.1	4.8 ± 1.8
	792	7	13.2 ± 3.1	5.0 ± 1.8
	920	6	13.6 ± 3.3	5.2 ± 1.9
	1065	6	14.4 ± 3.9	5.6 ± 2.0
298	26	20	4.9 ± 0.5	0.45 ± 0.15
	39	9	5.0 ± 0.7	0.50 ± 0.15
	52	12	5.7 ± 0.8	0.85 ± 0.25
	79	11	5.4 ± 0.7	0.71 ± 0.25
	92	7	6.1 ± 0.9	1.0 ± 0.3
	105	6	6.3 ± 1.2	1.1 ± 0.3
	131	31	7.5 ± 1.5	1.7 ± 0.5
	262	12	10.2 ± 2.0	2.9 ± 1.0
	393	15	9.0 ± 2.7	2.5 ± 1.3
	526	18	11.1 ± 2.7	3.5 ± 1.2
	526	10	11.0 ± 2.7	3.5 ± 1.2
	657	12	12.9 ± 3.3	4.5 ± 1.8
	792	12	11.2 ± 2.7	3.6 ± 1.2
	920	9	12.7 ± 2.9	4.4 ± 1.5
	1065	10	12.9 ± 2.9	4.5 ± 1.5
	1190	9	15.8 ± 3.8	5.9 ± 1.9
353	26	8	4.8 ± 0.7	0.38 ± 0.13
	52	7	5.8 ± 0.9	0.80 ± 0.25
	79	15	6.1 ± 1.1	1.0 ± 0.3
	105	10	6.8 ± 1.3	1.4 ± 0.4
	131	9	7.0 ± 1.1	1.5 ± 0.4
	262	10	8.8 ± 1.6	2.3 ± 0.6
	393	10	8.8 ± 2.4	2.4 ± 0.7
	521	9	10.0 ± 2.9	3.0 ± 1.0
	526	9	9.6 ± 2.8	2.7 ± 0.9
	657	8	10.8 ± 3.1	3.4 ± 1.1

The observed behavior of the OH decay following the flash photolysis of water vapor

$$\mathrm{H_2O} + h\nu\ (\lambda \geq 165\ \mathrm{nm}) \rightarrow \mathrm{OH}(X^2\Pi) + \mathrm{H}(1^2S)$$

can be explained by the sequence of reactions

$$\mathrm{OH} + \mathrm{OH}\ (+\mathrm{N_2}) \rightarrow \mathrm{H_2O_2}\ (+\mathrm{N_2}) \quad (1)$$

$$\mathrm{OH} + \mathrm{OH} \rightarrow \mathrm{H_2O} + \mathrm{O} \quad (2)$$

$$\mathrm{O} + \mathrm{OH} \rightarrow \mathrm{O_2} + \mathrm{H} \quad (3)$$

$$\mathrm{OH} + \mathrm{H}\ (+\mathrm{N_2}) \rightarrow \mathrm{H_2O}\ (+\mathrm{N_2}) \quad (4)$$

$$\mathrm{OH} + \text{wall} \rightarrow \text{products} \quad (5)$$

$$\mathrm{H} + \text{wall} \rightarrow \text{products} \quad (6)$$

Assuming a steady-state concentration of oxygen atoms and neglecting wall reactions (for total reaction times $\leq$ 3 ms), we obtain

$$-\mathrm{d}[\mathrm{OH}]/\mathrm{d}t = (3k_2 + 2k_{1,\mathrm{N_2}})[\mathrm{OH}]^2 + k_{4,\mathrm{N_2}}[\mathrm{H}][\mathrm{OH}] \quad \text{(vii)}$$

where $k_{1,\mathrm{N_2}}$ and $k_{4,\mathrm{N_2}}$ are the effective second-order rate coefficients

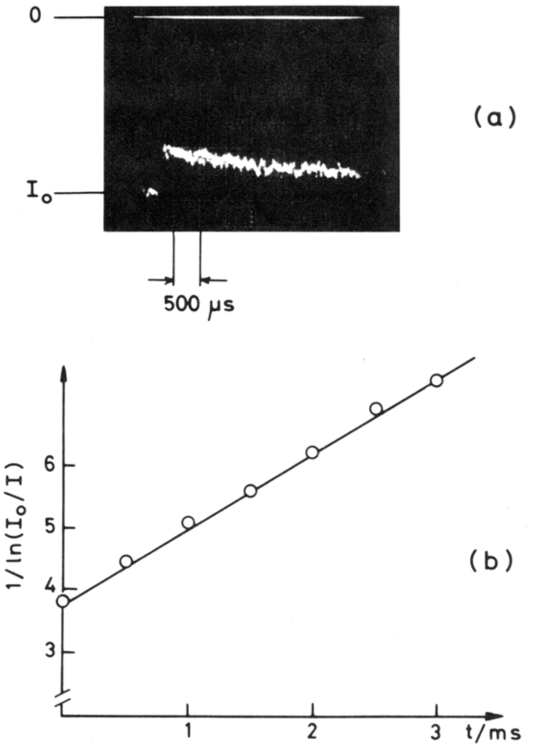

Figure 3. Experimental profile of OH absorption intensity vs time (a) and corresponding second-order kinetics analysis (b). $T = 298$ K, $p = 26$ mbar of N_2, $[OH]_0 = 7 \times 10^{13}$ cm^{-3}.

of reactions 1 and 4 for a given N_2 pressure. Due to the small H_2O partial pressure and because of the relative collision efficiencies of H_2O and N_2 (see below), the contribution of H_2O as a third body in reactions 1 and 4 can be neglected.

In order to extract the rate coefficient k_1, two aspects of eq vii have to be considered in some detail: (1) How has the pressure-independent reaction (2) to be separated from the pressure dependent reactions 1 and 4? (2) What is the contribution of reaction 4?

(1) In a previous publication on the OH + OH disproportionation reaction (2) and its temperature dependence[8] we have shown that for total pressures of ≤ 70 mbar of N_2 the effective rate constant for the second-order decay of OH is to a good approximation given by $k_{\mathrm{eff}} \simeq 3k_2 + 2k_{1,\mathrm{N}_2}$. Therefore, k_2 is simply obtained from linear extrapolation of k_{eff} against $p = 0$, with the result that $k_2 = (1.1 \pm 0.2) \times 10^{-12}$, $(1.3 \pm 0.15) \times 10^{-12}$, and $(1.4 \pm 0.2) \times 10^{-12}$ cm^3/s at temperatures of 253, 298, and 353 K, respectively.[8]

(2) The influence of reaction 4 and its contribution to k_{eff} are more difficult to assess. Only some qualitative aspects are obvious. Provided the initial rate of reaction 4 is slower than that of reactions 1 and 2, OH radicals will be consumed much faster than H atoms. As a consequence, the relative contribution of reaction 4 will *increase* with increasing reaction time and the overall OH decay will assume departures from second-order kinetics. In the limit $[H] \simeq [H]_0 = [OH]_0$ eq vii can be solved explicitly to yield

$$\frac{1}{[\mathrm{OH}]} = -\frac{a}{b} + \left[\frac{a}{b} + \frac{1}{[\mathrm{OH}]_0}\right]\exp(bt) \qquad \text{(viii)}$$

where $a = 3k_2 + 2k_{1,\mathrm{N}_2}$ and $b = k_{4,\mathrm{N}_2}[\mathrm{OH}]_0$. Hence, the deviation from second-order kinetics increases exponentially with reaction time, initial OH concentration and, of course, the magnitude of k_{4,N_2}. For small values of bt, i.e., short reactin times, and for low initial OH concentrations, the exponential term may be expanded, whereupon eq viii reduces to

$$\frac{1}{[\mathrm{OH}]} = (3k_2 + 2k_{1,\mathrm{N}_2} + k_{4,\mathrm{N}_2})t + \frac{1}{[\mathrm{OH}]_0} \qquad \text{(ix)}$$

and the OH decay assumes pure second-order kinetics with the weighted sum of all rate coefficients as the only term of the decay constant.

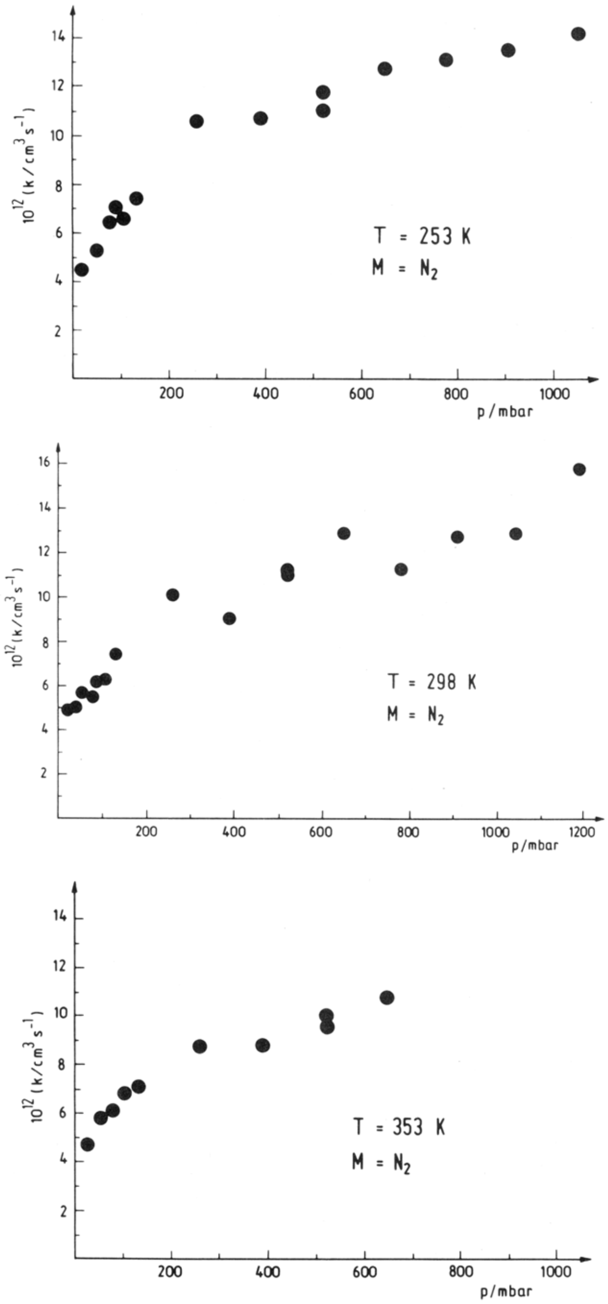

Figure 4. Effective second-order rate coefficients for total decay of OH as a function of N_2 pressure and at different temperatures.

In the present experiments departures from second-order kinetics were not observed. However, according to the above analysis and because such departures may easily be obscured by insufficient experimental signal-to-noise ratio, this in itself is no proof that reaction 4 can be discarded.

The rate coefficient for reaction 4 has previously been determined in our laboratory by use of a flow system technique. For the pressures applied in these experiments ($p \leqslant 15$ mbar) the reaction was found to be in the third-order limit with $k_4^0 = 4.8 \times 10^{-31}$ cm^6/s for M = N_2 and at 298 K.[15] With this value and with the assumption that k_4 remains in the low-pressure limit over the whole region up to 500 mbar, contributions by k_{4,N_2} to the pressure-dependent term of eq ix between 20% at 50 mbar and 60% at 500 mbar are predicted. As a result of these contributions, the remaining k_{1,N_2} values pass through a maximum, which is

---

(15) Zellner, R.; Erler, K.; Field, D. *16th Symposium (International) on Combustion*; The Combustion Institute: Pittsburgh, 1977; p 939.

physically unrealistic. Since the present work does not allow an independent determination of k_{4,N_2}, we can only seek for mutual consistency. This is possible by accepting (i) a falloff of k_{4,N_2} similar to the falloff of k_{1,N_2}, whereupon a 20% contribution of reaction 4 over the whole pressure region results, or (ii) a value of $k_4{}^0$ lower than previously reported. Since (i) is highly unlikely in view of the large high-pressure limiting rate coefficient (i.e., $k_4{}^\infty = 1.3 \times 10^{-10}$ cm³/s, as deduced from the D + OH isotope exchange reaction[16]), we are led to accept (ii) as the likely reason for inconsistency. The reduction of $k_4{}^0$ required in order to achieve consistency with the present work amounts to about a factor of 2 (i.e., $k_4{}^0 = 2.4 \times 10^{-31}$ cm⁶/s), whereupon the derived values for k_{1,N_2} regain their falloff behavior and the necessary corrections fall below 10% (25%) at pressures below 150 (1000) mbar. It should be noted that this requirement for $k_4{}^0$ is not beyond reasonable error limits of our flow system studies.

A further potential source of complication of the reaction system, which has so far been left unmentioned, arises from the reaction of OH with its recombination product

$$OH + H_2O_2 \rightarrow H_2O + HO_2 \tag{7}$$

followed by the fast reaction

$$OH + HO_2 \rightarrow H_2O + O_2 \tag{8}$$

Reaction 7 has a rate coefficient of $k_7 = 1.7 \times 10^{-12}$ cm³/s, equal in magnitude to k_1 at pressures of ~100 mbar of N_2. Its effect on the OH profile will be similar to that of reaction 4, i.e., to become noticeable only at longer reaction times (after sufficient H_2O_2 has built up) where it creates deviations from second-order kinetics. A simple estimate shows that at pressures of 100 mbar of N_2 and for OH conversions of 50% the contribution of reactions 7 and 8 to the instantaneous OH loss will be below 15%. In agreement with the experimental observations this is too low to be noticed via mixed reaction orders. It should be noted that due to the pressure dependence of k_1 the influence of reactions 7 and 8 is further alleviated with increasing pressure.

The resulting k_{1,N_2} values are listed in Table II. Due to other error limits which exceed the estimated influences of reactions 4, 7, and 8, the data presented are uncorrected for these reactions. It should be borne in mind though that they must be upper limits with a most probable systematic error not exceeding 25% at all pressures.

The data of Table II for pressures below ~100 mbar may be identified to correspond to the low-pressure limit where k_1 increases proportionally to [M] (cf. Figure 4), $k_{1,N_2} = k_{1,N_2}{}^0[M]$. The values then obtained for the third-order limiting rate coefficient are

$$k_{1,N_2}{}^0\ (T = 253\ \text{K}) = (9.1^{+1.8}_{-3.5}) \times 10^{-31}\ \text{cm}^6/\text{s}$$

$$k_{1,N_2}{}^0\ (T = 298\ \text{K}) = (6.9^{+1.4}_{-2.5}) \times 10^{-31}\ \text{cm}^6/\text{s}$$

$$k_{1,N_2}{}^0\ (T = 353\ \text{K}) = (6.2^{+1.3}_{-2.3}) \times 10^{-31}\ \text{cm}^6/\text{s}$$

The different error limits take into account the uncorrected contribution of reaction 4.

III.1.2. M = H₂O. Since water vapor, albeit in small concentrations, was used in all experiments as a source of OH radicals and because H_2O is a common constituent in reaction environments at both low and high temperatures, we have performed separate experiments to determine the rate coefficient for OH recombination with H_2O as a third body. Due to vapor pressure limitations, however, the accessible pressure range was limited. In fact we have chosen to study reaction mixtures of N_2 and H_2O with a constant H_2O mole fraction of $x_{H_2O} = 0.11$ at temperatures of 298 and 353 K. Experimental conditions and results are summarized in Table III. Figure 5 is a graphical representation of the data, together with the results obtained for pure N_2 as a third body. It should be noted that in the derivation of these data the influence of H_2O on the pressure broadening of the OH absorption line has been neglected.

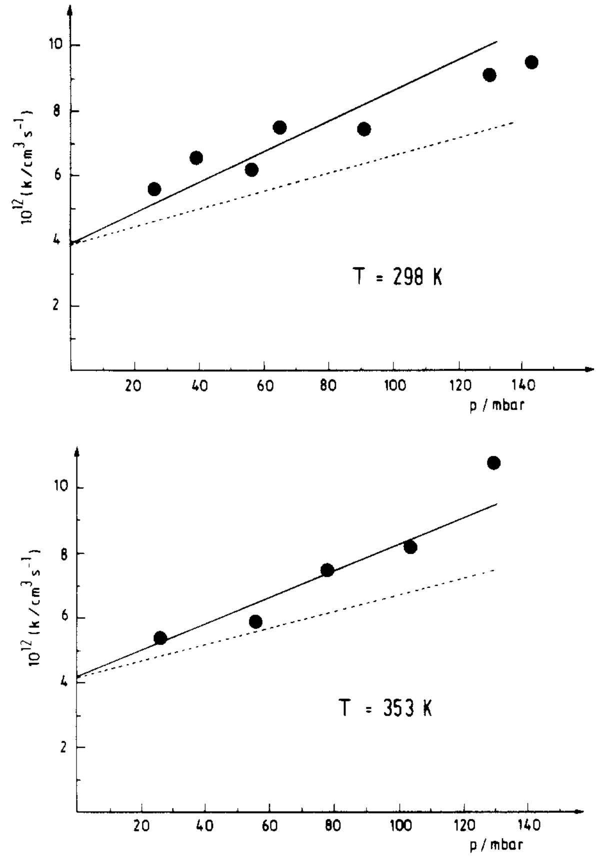

Figure 5. Effective second-order rate coefficients for total decay of OH as a function of total pressure of mixtures containing 11% H_2O in N_2 for T = 298 and 353 K. The dotted lines represent the corresponding results in pure N_2.

TABLE III: Summary of Experimental Conditions and Results for Mixtures of N_2 and H_2O (x_{H_2O} = 0.11)

T/K	p^a/mbar	no. expt	$10^{12}k_{\text{eff}}$/cm³ s⁻¹
298	26	7	5.6 ± 1.5
	39	6	6.6 ± 1.7
	56	7	6.2 ± 1.8
	65	8	7.5 ± 2.0
	91	7	7.4 ± 2.0
	130	8	9.1 ± 2.6
	143	6	9.5 ± 2.6
353	26	6	5.4 ± 1.4
	56	7	5.8 ± 1.6
	78	8	7.5 ± 1.3
	104	7	8.2 ± 1.8
	136	6	10.8 ± 2.7

[a] Total pressure ($P_{N_2} + P_{H_2O}$).

The overall rate coefficients of Table III may be identified with

$$k_{\text{eff}} = 3k_2 + 2k_{1,N_2} + 2k_{1,H_2O} \tag{x}$$

where k_{1,N_2} and k_{1,H_2O} are the effective rate coefficients for reaction 1 for the experimental partial pressures of N_2 and H_2O. Since for $p \leq 100$ mbar, k_1 may be assumed to be in the low-pressure limit and since $x_{H_2O} = 0.11$, the pressure-dependent part of eq x is identical with

$$k_{\text{eff}} - 3k_2 = 2(k_{1,N_2}{}^0 + 0.11k_{1,H_2O}{}^0)[N_2] \tag{xi}$$

Hence, $k_{1,H_2O}{}^0$ may be derived from the slope of the plots of Figure 5 where $[N_2]$ is connected with the total pressure (p_{tot}) via $[N_2] = (6.53 \times 10^{-18})p_{\text{tot}}/T$. We obtain

$$k_{1,H_2O}{}^0\ (T = 298\ \text{K}) = (4.0^{+1.3}_{-2.0}) \times 10^{-30}\ \text{cm}^6/\text{s}$$

$$k_{1,H_2O}{}^0\ (T = 353\ \text{K}) = (4.1^{+1.3}_{-2.0}) \times 10^{-30}\ \text{cm}^6/\text{s}$$

---

(16) Margitan, J. J.; Kaufman, F.; Anderson, J. G. *Chem. Phys. Lett.* **1975**, *34*, 485.

corresponding to a relative collision efficiency for H_2O and N_2 of about 6 at both temperatures. A temperature dependence of $k_{1,H_2O}{}^0$ could not be deduced.

III.2. Comparison with Theoretical Predictions and Other Experimental Data. The interaction of two $OH(^2\Pi_{3/2,1/2})$ radicals gives rise to a total of eight surfaces, four triplet and four singlet. Reaction on the lowest triplet surface leads adiabatically to atomic oxygen and water via the direct abstraction mechanism[8]

$$OH(^2\Pi) + OH(^2\Pi) \rightarrow H_2O(^1A_1) + O(^3P) \qquad (2)$$

while reaction on the singlet surfaces leads to the recombination product, hydrogen peroxide, viz.

$$OH(^2\Pi) + OH(^2\Pi) \rightarrow H_2O_2(^1A) \qquad (1)$$

The four singlet surfaces (two $^1A'$ and two $^1A''$) differ in the orientations of the singly occupied oxygen atom orbitals and the doubly occupied oxygen lone pair orbitals relative to each other.[17] Recent ab initio calculations[17] indicate that there is a strong interaction of these surfaces with variable importance depending on the angle of the OOH moiety during the approach of the two OH radicals and resulting in a complex recombination reaction pathway. Whereas these calculations confirm the adiabaticity of reaction 1, its details reach far beyond the information obtained in the present thermal experiment.

III.2.1. The Low-Pressure Limit. The present experiments have essentially been carried out at and near the low-pressure limit of recombination. Therefore, this regime deserves some detailed consideration. Both theoretical and other experimental information are available for comparison.

Using detailed molecular properties of H_2O_2 to calculate the distribution function of vibrationally excited states, Troe[18] has derived the rate coefficient for recombination in the strong collision limit. At $T = 300$ K and for M = Ar a value of $k_{1,Ar}{}^{0,sc} = 1.5 \times 10^{-30}$ cm^6/s was obtained. Correcting for the M dependence of the Lennard-Jones collision frequency,[17] the corresponding value for M = N_2 is predicted to be $k_{1,N_2}{}^{0,sc} = 1.6 \times 10^{-30}$ cm^6/s. This value may be compared with the present experimental result ($k_{1,N_2}{}^0$) by introducing the collision efficiency β_c, viz.

$$k_1{}^0 = \beta_c k_1{}^{0,sc} \qquad (xii)$$

With $k_{1,N_2}{}^0 = 6.9 \times 10^{-31}$ cm^6/s at 298 K we obtain $\beta_{c,N_2} = 0.43$, in agreement with collision efficiencies observed for N_2 as a third body in various recombination reactions forming products of comparable complexity.[19] According to the definition of β_c, viz.[18]

$$\beta_c/(1 - \beta_c{}^{1/2}) \simeq \langle \Delta E \rangle / kT$$

$\beta_{c,N_2} = 0.43$ corresponds to an average energy transferred in collision with N_2 of 3.7 kJ/mol.

The first experimental investigation of reaction 1 at room temperature was performed by Black and Porter[9] using absorption spectrometry in the flash photolysis of H_2O vapor. Due to insufficient knowledge about the prevailing OH concentrations, this work provided mainly relative rates for various third bodies including Ar, N_2, and H_2O. In a subsequent study, using a similar technique, Caldwell and Back[10] monitored the yields of H_2 and O_2 and determined the relative rates of reactions 1 and 2. By combination with the relative third-body efficiencies as determined by ref 9 and with the absolute value of k_2 as obtained by Del Greco and Kaufman[1] ($k_2 = 1.4 \times 10^{-12}$ cm^3/s, in good agreement with our more recent result[8]), a value of $k_{1,N_2}{}^0 = 1.7 \times 10^{-30}$ cm^6/s, a factor of 2.4 larger than the present result, was derived. Since this value exceeds the theoretical strong collision limit, it should probably be discarded. Likely sources of error in the study of ref 10 have previously been discussed.[7]

The only previous direct study of reaction 1 at room temperature was performed by Trainor and von Rosenberg[7] using a technique

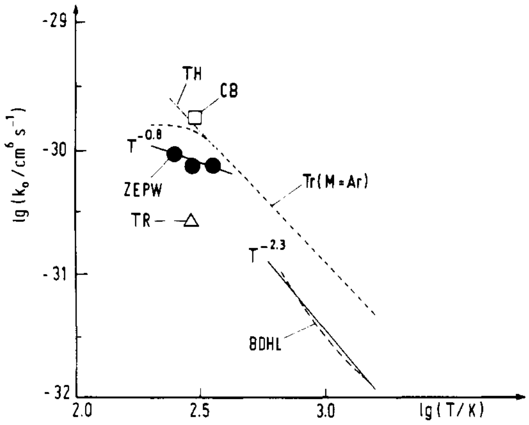

Figure 6. Temperature dependence of the low-pressure limiting rate coefficient for $OH + OH + N_2 \rightarrow H_2O_2 + N_2$. CB, Caldwell and Back;[10] TR, Trainor and von Rosenberg;[7] BDHL, Baulch et al.[25] (evaluation based on high-temperature dissociation data); Tr, Troe[18] (theoretical strong collision limit, M = Ar); TH, Tsang and Hampson[26] (strong collision limit, derived from expression for high-temperature dissociation rate coefficient); ZEPW, this work.

essentially similar to ours. From measurements in up to 500 mbar of N_2 a low-pressure limiting rate coefficient of $k_{1,N_2}{}^0 = (2.5 \pm 0.3) \times 10^{-31}$ cm^6/s was derived. Although the experimental data show a substantial amount of scatter, we have no obvious explanation why this result falls a factor of 2.7 below our data. We can only speculate that the lower value is caused by either (or a combination) of the following two reasons: (i) an unrecognized falloff behavior and (ii) inhomogeneous OH distributions along the optical path due to perpendicular arrangement of flash lamps and OH detection path. Both these potential error sources are excluded in the data analysis and experiment, respectively, of the present work. A comparison of the various determinations of $k_{1,N_2}{}^0$ is presented in Figure 6.

A quantity of formidable interest next to the absolute value of $k_{1,N_2}{}^0$ is its temperature dependence. The results from our experiments at 253, 298, and 353 K, if represented in T^{-n} form (cf. Figure 6), are consistent with $n = 0.8$. Unfortunately, there are no other temperature-dependent data in the low-temperature region that our result can be compared with. However, on the basis of experimental results of the dissociation of H_2O_2 in the temperature range 700–1200 K[20-24] Baulch et al.[25] have recommended the expression $k_{1,N_2}{}^0 = (2.5 \times 10^{-33}) \exp(2550K/T)$ cm^6/s. This expression, if converted to T^{-n}, corresponds to $n = 2.3$ and extrapolates well to our data around room temperature (cf. Figure 6). Hence, dissociation and recombination data must be considered consistent. The weaker temperature dependence of our low-temperature data is not contradictory, since a strong decrease of n in the low-temperature region is also predicted for the theoretical strong collision limit[18] and some curvature of the log k vs log T plot is to be expected (cf. Figure 6). The expression $k_{1,N_2}{}^0 = (2.9 \times 10^{-25})T^{-2.13}$ cm^6/s recently recommended for the strong collision limit by Tsang and Hampson[26] does not take any account of this effect and therefore should not be used at lower temperatures ($T \leq 350$ K).

The recombination of OH radicals at 298 in the presence of H_2O as a third body has to our knowledge never before been determined directly. However, our result ($k_{1,H_2O}{}^0 = 4.0 \times 10^{-30}$ cm^6/s) when taken relative to $k_{1,N_2}{}^0$ ($k_{1,H2O}{}^0/k_{1,N_2}{}^0 = 5.7$) is in

---

(17) Harding, L. B., unpublished results, cited in the Annual Report of the Theoretical Chemistry Group, Argonne National Laboratory, Argonne, IL, 1987.

(18) Troe, J. *J. Chem. Phys.* **1977**, *66*, 4758.

(19) Patrick, R.; Golden, D. M. *Int. J. Chem. Kinet.* **1983**, *15*, 1189.

(20) McLane, C. K. *J. Chem. Phys.* **1949**, *17*, 379.

(21) Giguère, P. A.; Liu, I. D. *Can. J. Chem.* **1957**, *35*, 283.

(22) Satterfield, C. N.; Stein, T. W. *J. Phys. Chem.* **1957**, *61*, 537.

(23) Hoare, D. E.; Protheroe, J. B.; Walsh, A. D. *Trans. Faraday Soc.* **1959**, *55*, 548.

(24) Baldwin, R. R.; Brattan, D. *8th Symposium (International) on Combustion*; The Combustion Institute: Pittsburgh, 1960; p 110.

(25) Baulch, D. L.; Drysdale, D. D.; Horne, D. G.; Lloyd, A. C. *Evaluated Kinetic Data for High Temperature Reactions*; Butterworths: London, 1972; Vol. 1.

(26) Tsang, W.; Hampson, R. F. *J. Phys. Chem. Ref. Data* **1986**, *15*, 1087.

excellent agreement with the relative study of Black and Porter[9] ($k_{1,H_2O}/k_{1,N_2} = 5.5$). Hence there is little doubt that, as expected, H_2O is a much more efficient collider than N_2. In order to compare with theoretical predictions we may again use the result of Troe[18] which in combination with a corrected Lennard-Jones collision number yields $k_{1,H_2O}{}^{0,sc} = 2.3 \times 10^{-30}$ cm^6/s for the theoretical strong collision low-pressure limiting rate coefficient. This is a factor of 1.7 lower than the experimental result and in conflict with eq xii since β_c (per definition) cannot exceed unity. Although this disagreement is within the combined acceptable error limits, the larger experimental value may be taken as indicative of a complex formation mechanism of recombination rather than an energy-transfer mechanism which is the basis of the theoretical calculation. Proof for such a mechanism can only come from the temperature dependence of the $OH + OH + H_2O \rightarrow H_2O_2 + H_2O$ reaction at lower temperatures which should clearly exceed the one observed with N_2. The present work is insufficient to draw such conclusions.

III.2.2. Falloff Behavior and the High-Pressure Limit. Although our experiments refer primarily to the low-pressure limit, a falloff behavior of the rate coefficients at higher pressures is clearly observed (cf. Figure 4). Therefore an attempt can be made to describe the falloff quantitatively and to extract a high-pressure limiting rate coefficient. According to Troe and co-workers,[27,28] the rate coefficient for recombination in the falloff region can be represented conveniently in reduced and symmetrical form by

$$\frac{k}{k^\infty} = \left(\frac{k^0[\mathrm{M}]/k^\infty}{1 + k^0[\mathrm{M}]/k^\infty}\right) F_{\mathrm{cent}}{}^{\mathrm{sc}\{1 + [\log (k^0[\mathrm{M}]/k^\infty)/N_{\mathrm{sc}}]^2\}^{-1}} \qquad \text{(xiii)}$$

where $F_{\mathrm{cent}}{}^{\mathrm{sc}}$ is the broadening factor in the center of the falloff curve ($k^0[\mathrm{M}] = k^\infty$) and N_{sc} is the width of the falloff curve, given by $N_{\mathrm{sc}} \simeq 0.75 - 1.25 \log F_{\mathrm{cent}}{}^{\mathrm{sc}}$. In this expression weak collision effects have been neglected. The broadening factor $F_{\mathrm{cent}}{}^{\mathrm{sc}}$ can be calculated from the $H_2O_2{}^*$ transition-state frequencies via the Kassel parameters S_K and B_K.[28] Since these are unknown (without prior knowledge of k^∞), we have chosen to make an estimate based on the frequency pattern of the H_2O_2 molecule. Using this approach, we obtain at 298 K $S_K = 1 + U^*/kT \simeq 3$, whereupon $F_{\mathrm{cent}}{}^{\mathrm{sc}} \simeq 0.6$.[29] Together with k^0, which is known from the experiment, we can now construct reduced falloff curves from eq xiii using k^∞ as a parameter. The best fit with the experiment is then obtained for a high-pressure limiting rate coefficient of

$$k_1{}^\infty = 1.5 \times 10^{-11} \text{ cm}^3/\text{s}$$

A comparison of calculated and experimental falloff behaviors of k_1 is presented in Figure 7. This figure also contains the theoretical strong collision limit[18] as well as a falloff calculation with $F_{\mathrm{cent}}{}^{\mathrm{sc}} = 0.8$. The latter does not provide an equally satisfactory fit to the experimental data, unless a smaller $k_1{}^\infty$ value ($\sim 8 \times 10^{-12}$ cm^3/s) is chosen.

The high-pressure limiting rate coefficient $k_1{}^\infty$ has to our knowledge not been determined before such that no data are available for direct comparison. However, Brouwer et al.[30] have recently presented a calculation of specific rate coefficients $k(E,J)$ for the dissociation of H_2O_2 using the statistical adiabatic channel (SAC) model. Their result is in agreement with measurements of state-resolved dissociation rates in vibrational overtone excitation experiments.[31] Moreover, calculations of the high-pressure limiting rate coefficient for the thermal reaction are found to be entirely consistent with the present result for the reverse recombination.

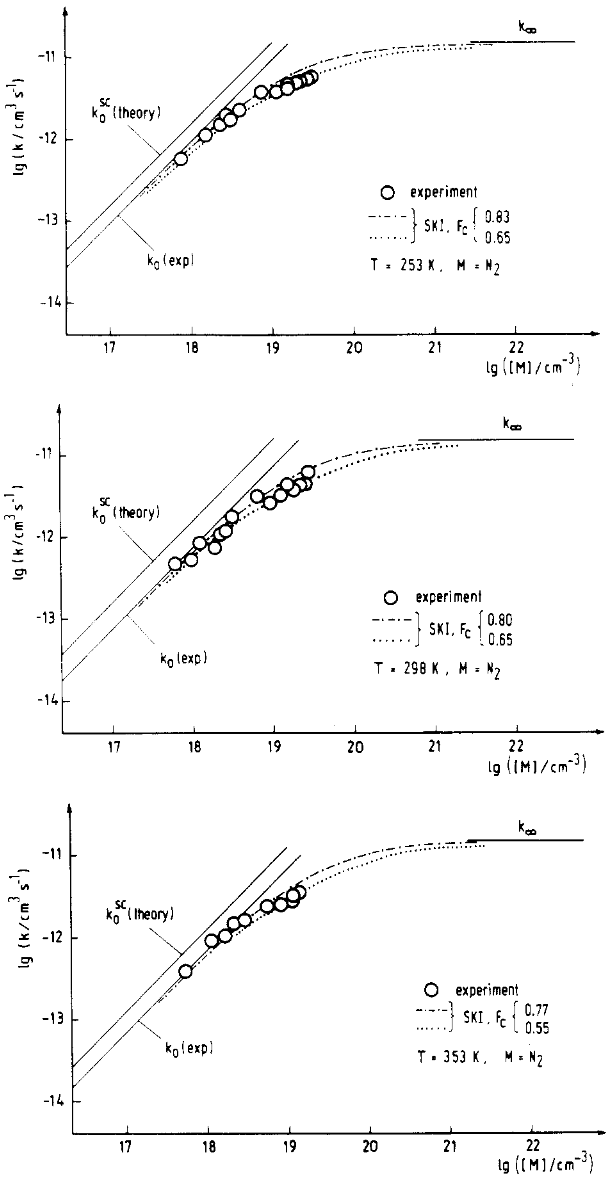

Figure 7. Comparison of calculated falloff curves for $OH + OH\ (+N_2) \rightarrow H_2O_2\ (+N_2)$ with experimental data for T = 253, 298, and 353 K. The theoretical k^0 lines are for the strong collision limit.[18]

Figure 7 also shows the corresponding comparison between calculated and experimental falloff for 253 and 353 K. In order to perform the calculation using eq xiii the temperature dependence of $F_{\mathrm{cent}}{}^{\mathrm{sc}}$ was derived according $F_{\mathrm{cent}}{}^{\mathrm{sc}}(T) \simeq \exp(-T/T^*) + \exp(-4T^*/T)$,[28] whereupon we obtain $F_{\mathrm{cent}}{}^{\mathrm{sc}} = 0.65$ and 0.55 at T = 253 and 353 K, respectively. With these data a satisfactory agreement with the experiments at both temperatures is again obtained with $k_1{}^\infty = 1.5 \times 10^{-11}$ cm^3/s. Hence, we conclude that $k_1{}^\infty$ is not, or at least not strongly, temperature dependent. While this is generally expected, a more stringent confirmation is provided by the detailed SAC model calculation[30] from which $k_1{}^\infty(T) \simeq T^{-0.37}$ is predicted.

Acknowledgment. We gratefully acknowledge financial support of this work by "Fonds der Chemischen Industrie". R.Z. thanks the "Deutsche Forschungsgemeinschaft" for a "Heisenberg-Stipendium". Valuable discussion of this work with Prof. J. Troe is gratefully acknowledged.

Registry No. OH, 3352-57-6; N_2, 7727-37-9; H_2O, 7732-18-5.

---

(27) Luther, K.; Troe, J. *17th Symposium (International) on Combustion*; The Combustion Institute: Pittsburgh, 1979; p 535.

(28) Troe, J. *Ber. Bunsen-Ges. Phys. Chem.* **1983**, *87*, 161. Troe, J. *J. Phys. Chem.* **1979**, *83*, 114.

(29) Ewig, F. Dissertation, Universität Göttingen, 1987.

(30) Brouwer, L.; Cobos, C. J.; Troe, J.; Dübal, H. R.; Crim, F. F. *J. Chem. Phys.* **1987**, *86*, 6171.

(31) Dübal, H. R.; Crim, F. F. *J. Chem. Phys.* **1985**, *83*, 3863.